

END-TO-END CRYSTAL STRUCTURE PREDICTION FROM POWDER X-RAY DIFFRACTION

Qingsi Lai^{1,2}, Lin Yao^{1,*}, Zhifeng Gao¹, Siyuan Liu¹, Hongshuai Wang¹,
Shuqi Lu¹, Di He³, Liwei Wang^{2,3}, Cheng Wang^{4,5} and Guolin Ke^{1,*}

¹ DP Technology, Beijing, 100080, China

² Center for Data Science, Peking University, Beijing 100871, China

³ School of Intelligence Science and Technology, Peking University, Beijing 100871, China

⁴ College of Chemistry and Chemical Engineering, Xiamen University, Xiamen, 361005, China

⁵ AI for Science Institute, Beijing, 100084, China

ABSTRACT

Powder X-ray diffraction (PXRD) is a crucial means for crystal structure determination. Such determination often involves external database matching to find a structural analogue and Rietveld refinement to obtain finer structure. However, databases may be incomplete and Rietveld refinement often requires intensive trial-and-error efforts from trained experimentalists, which remains ineffective in practice. To settle these issues, we propose XtalNet, the first end-to-end deep learning-based framework capable of ab initio generation of crystal structures that accurately match given PXRD patterns. The model employs contrastive learning and Diffusion-based conditional generation to enable the simultaneous execution of two tasks: crystal structure retrieval based on PXRD patterns and conditional structure generations. To validate the effectiveness of XtalNet, we curate a much more challenging and practical dataset hMOF-100, XtalNet performs well on this dataset, reaching 96.3% top-10 hit ratio on the database retrieval task and 95.0% top-10 match rate on the ranked structure generation task.

1 Introduction

Simulating or experimentally deriving powder X-ray diffraction (PXRD) patterns [1] from crystal structures is a well-established procedure. PXRD analysis is widely utilized for the prediction of material properties, (such as crystalline phases, orientation, lattice parameters, and grain size), as well as for the identification of crystal structures. For instance, upon crystal synthesis, comparing experimental PXRD patterns of unknown materials against databases like the International Center for Diffraction Data (ICDD) and the Inorganic Crystal Structure Database (ICSD) [2] helps identify structural analogues. Then Rietveld refinement [3] is employed for refining roughly analogous structures incrementally to achieve greater precision.

However, issues with incomplete data and inconsistencies in database matching can result in structures that are less applicable to real-world scenarios. Additionally, the substantial amount of trained experimentalists manual efforts are required during Rietveld refinement, which makes the overall process time-consuming and labor-intensive. There have been efforts to resolve these problems, some methods attempts to classify structures based on PXRD in a deep learning way [4, 5, 6]. However, these methods have not fundamentally resolved the issue, as they merely yield broad crystal classifications rather than specific structures. Consequently, this necessitates the direct prediction of crystal structures based on the given PXRD data as condition, without other reliance like external databases. Nevertheless, the ab initio prediction or generation of structures from PXRD patterns remains an unrealized goal.

Setting aside the conditional crystal structure prediction (CSP) based on PXRD, the state of unconditional CSP remains in its early stages. Research has demonstrated that deep learning can to some extent supplant Density Functional Theory (DFT) [7], while requiring less computational time. These methods generally take basic parameters, such as

* These authors should be considered co-corresponding authors.

the type and number of atoms, as pre-defined information before embarking on structure prediction. Many successful models have utilized diffusion-based approaches, including the Crystal Diffusion Variational Autoencoder (CDVAE) [8] and DiffCSP [9], which have delivered promising results. These models are carefully designed to account for the unique periodicity and equivariance challenges in crystal structure prediction. However, most of these studies have been conducted using simplified datasets, such as Perov-5 [10, 11], MP-20 [12] and Carbon-24 [13, 14], which contain a limited number of atoms (up to 5, 20, and 24 atoms respectively) in a single unit cell. This limitation results in a reduced conformational search space and decreases the ambiguity in potential solutions, thereby improving model performance. The efficacy of these methods in predicting more complex structures or under stringent conditions has yet to be validated. However, real-world applications often require the prediction of more complex material structures under certain conditions, such as PXRD. This area remains largely unexplored in current research.

Despite the relatively underdeveloped state of diffusion model in conditional CSP, their conditional counterparts have been successfully implemented in the text-to-image generation domain, with prominent examples such as Stable Diffusion [15]. These models employ text embeddings generated by pretrained CLIP [16] text encoder to guide the diffusion process in generating images conditioned on textual descriptions. Drawing inspiration from the success models, we have explored the potential of integrating a contrastive learning approach and a DDPM into our conditional crystal structure prediction methodology. Since the similarity between PXRD-crystal and text-image, the same contrastive PXRD-crystal pre-training strategy can also be applied to guide the generation of crystal structures based on PXRD pattern.

Therefore, we propose **XtalNet** derived from PXRD-crystal, which primarily consists of a contrastive PXRD-crystal pre-training (CPCP) module and a conditional crystal structure generation (CCSG) module. The CPCP module can carry out database retrieval tasks, achieving a top-10 hit ratio of 96.3%. Furthermore, by utilizing CCSG modules, multiple candidate crystal structures can be generated conditioned on PXRD pattern. Subsequently, these candidate structures are scored and ranked using the CPCP module, thus accomplishing the ranked structure generation task with a top-10 match rate of 95% and an RMSE of 0.3985.

Our research strives to extend the capabilities of deep learning in generating crystal structures based on PXRD pattern, encompassing more complex structure and specific conditions. Our primary contributions are as follows:

- We present the first end-to-end deep learning based method for conditional crystal structure generation and identification based on PXRD patterns that operates independently of human intervention, databases or other external dependencies, which is a departure from traditional approaches.
- We pioneer the conditional generation of crystal structures for complex materials with atomic counts achieving 100. Previous studies have focused on unconditional material generation, making our exploration significant for the generation of novel materials under specific conditions.
- Our approach achieves a noteworthy level of performance without reliance on specialized external resources. For database retrieval task, the top-10 hit ratio has reached 96.3%. For ranked structure generation, the top-10 match rate and RMSE have reached 95% and 0.3985, respectively.

2 Results

2.1 Overview of XtalNet

XtalNet is primarily composed of two parts as shown in Figure 1: one is the Contrastive PXRD-crystal pretraining (CPCP) module, and the other is conditional crystal structure generation (ccsg) module based on conditional diffusion. CPCP module is mainly utilized for database retrieval tasks, which aims to derive the most similar crystal structure based on known PXRD pattern. While CCSG module is designed for recover the crystal structure according to a given PXRD pattern.

CPCP module adopts a design similar to CLIP[16]. A transformer-based PXRD feature extractor is utilized to extract PXRD features. Subsequently a crystal structure feature network based on Equivariant Graph Neural Networks is employed to extract crystal structure features. Similarity scores are obtained by the cosine similarity between PXRD features and crystal structure features. Matching pairs of PXRD pattern and corresponding crystal structure are considered as positive pair, whereas non-matching pairs are regarded as negative pair. Then infoNCE loss function is adopted for contrastive learning training.

CCSG module mainly uses diffusion-based framework, while the PXRD feature is utilized as a critical condition for generation. The noised crystal structure, the PXRD feature and time embedding are taken by crystal structure network to denoise on fractional coordinate and lattice. The PXRD feature extractor is initialized by CPCP module pretraining, which is important for generation performance.

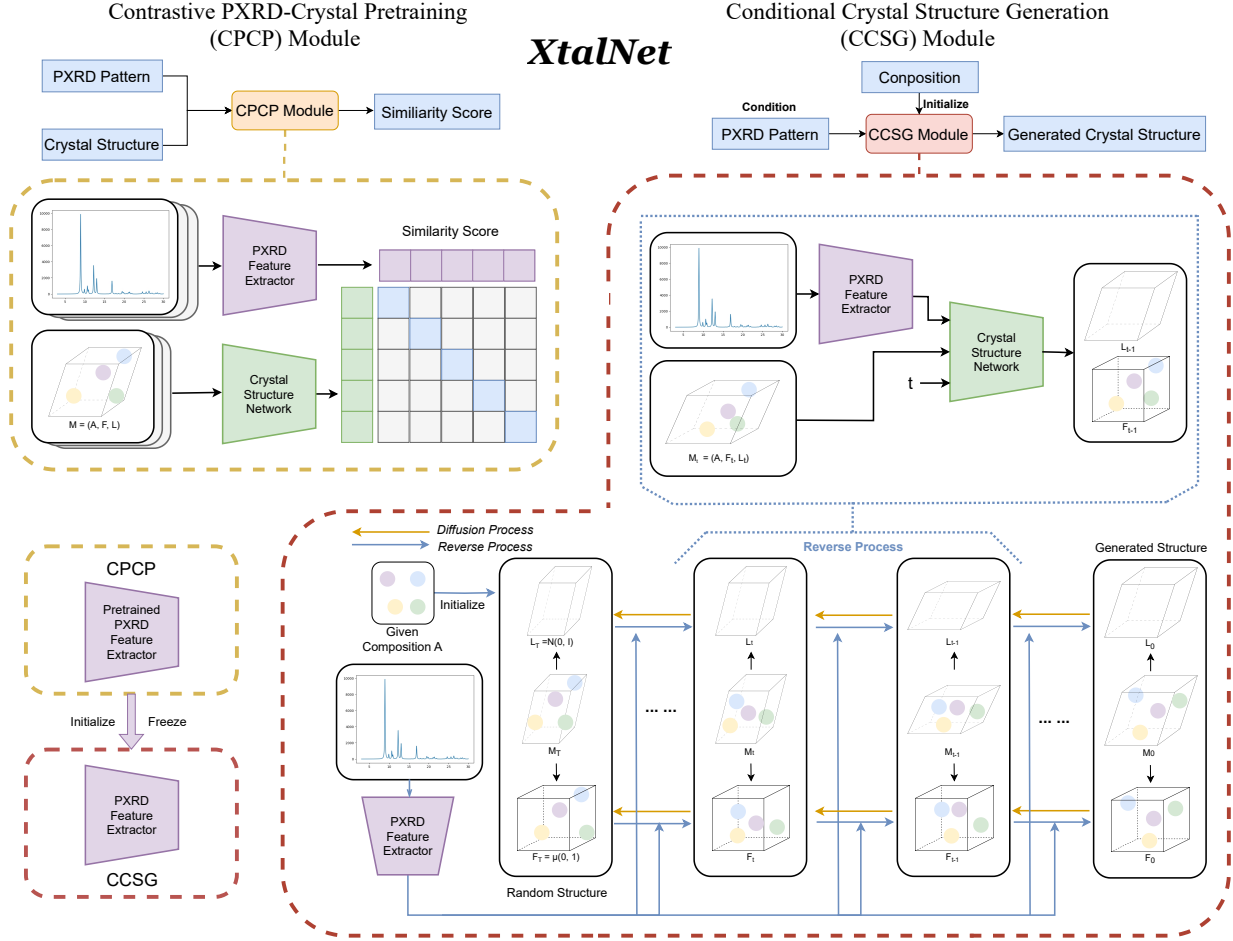


Figure 1: **Architecture of XtalNet.**

2.2 Dataset Preparing and Evaluation Metrics

We curate a MOFs dataset named hMOF-100 based on hypothetical MOFs (hMOFs) [17]. We follow Uni-MOF [18] splitting, then filter each split to retain only materials with 100 or fewer atoms in the unit cell to construct train (73,332), validation (9,117) and test (9,081) set. As the original hMOFs database does not have PXRD patterns, we calculate the simulated PXRD pattern for every crystal in hMOF-100 by GSAS[19]. Each PXRD pattern is simulated with 2θ angle from 3° to 30° with a step size of 0.02° . Considering that only the relative intensities of PXRD patterns carry practical meaning, we normalized the intensity of each pattern by dividing it by its maximum value.

For database retrieval task, we use the top- k hit ratio as the metrics, which measures how often the desired crystal structures are found. Following the previous works[8, 9], we evaluated the ranked structure generation task by Match Rate and RMSE. Specifically, Match Rate is the proportion of the matched generated structure over all ground truth while the StructureMatcher class in pymatgen [20] with thresholds $stol=0.7$, $angle_tol=5$, $ltol=0.2$ is used. RMSE is calculated between matched structure and ground truth normalized by $\sqrt[3]{V/N}$, where V and N is the volume of lattice and atom numbers in the unit cell respectively.

2.3 Embedding Validation via Database Retrieval

In order to validate the effectiveness of embedding trained from CPCP module, we design the database retrieval task which aims at searching for crystal structures based on a known PXRD pattern. Initially, a PXRD pattern and a database containing numerous crystal structures are known. Our objective is to utilize the embedding induced from the PXRD pattern to identify and retrieve the crystal structure that most closely corresponds to the given PXRD pattern.

Specifically, a total of 9,081 crystal structure embeddings from the test sets were compiled by crystal structure network to create a retrieval database. Searches were conducted using PXRD embeddings created by PXRD feature extractor as query keys, leveraging cosine similarity as the search criterion. The search outcomes are summarized in Table 1. The top-10 hit ratio has reached 96.3% among 9,081 cases, which means the information space of PXRD pattern has been aligned well with crystal structure space.

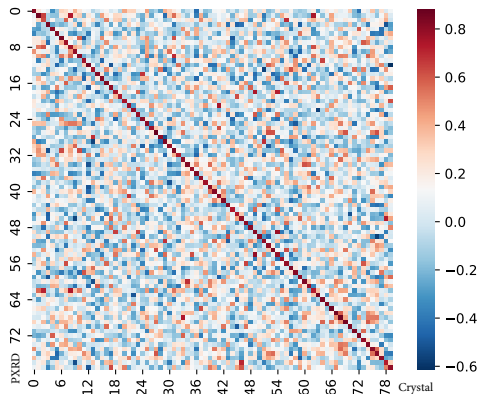


Figure 2: Heat map of similarity score between PXRD pattern and crystal structure.

Table 1: Results on database retrieval.

| | Top- k | | | |
|---------------|----------|------|------|------|
| | 1 | 3 | 5 | 10 |
| Hit Ratio (%) | 42.5 | 74.4 | 86.8 | 96.3 |

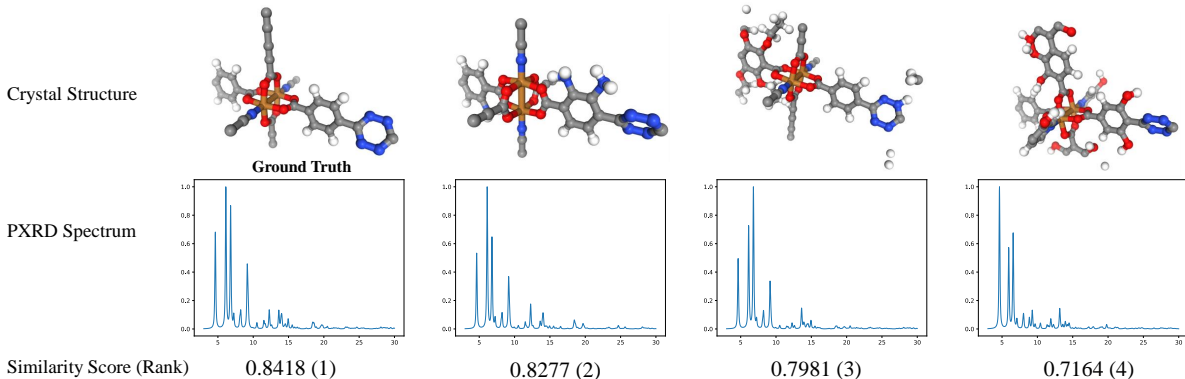


Figure 3: Visual analysis of database retrieval task.

To more intuitively observe the effectiveness of the retrieval, we randomly selected 80 crystal structures and their corresponding PXRD pattern and used their similarity scores to construct a heatmap as shown in Figure 2. In the heatmap, colors closer to red indicate higher similarity, while colors closer to blue indicate lower similarity. The diagonal of the heatmap represents the correctly matched pairs. It can be seen that there is a distinct red distribution along the diagonal, indicating that the model is capable of accurately identifying the crystal structures corresponding to the PXRD pattern.

We visualized a retrieval result of a given PXRD pattern. Four of the highest-scoring crystal structures retrieved by the system, their corresponding PXRD pattern alongside their similarity score and rank are shown in Figure 3. It is observable that the Non ground truth structures with higher similarity scores possess similar metal-connecting structures, and the connected ligands also exhibit a high degree of similarity. From the perspective of the PXRD spectra, the peak positions of the high-intensity peaks in the PXRD spectra corresponding to similar structures also show high similarity. Therefore, our retrieval model is capable of effectively extracting high-level information corresponding to the structures from the PXRD spectra, laying a foundation for the subsequent generation model.

2.4 Ranked Structure Generation

The task of Ranked Structure Generation is a more intricate process that consists of two stages. In the first stage, CCSG module is employed to generate N crystal structures. The second stage involves the use of CPCP module mentioned above to calculate the similarity score between the target PXRD pattern and the generated crystal structures, thereby

enabling ranking. Through this process, we obtain crystal structures with a ranked preference. Subsequently, evaluation is conducted on the top- k ranked crystal structures.

Specifically, 80 PXRD patterns are randomly selected from test set, then 20 potential crystal structures under each PXRD pattern are generated by CCSG module. These structures were then ranked based on cosine similarity between the PXRD embeddings and the embeddings of the generated candidates. The rankings reflect the confidence in each structure’s match to the PXRD pattern. Then the top- k ranked candidate structures can be compared with ground truth to compute metrics. Performance metrics for this process are detailed in Table 2. The match rate of top-10 candidates has achieve 95%, which indicate that XtalNet is capable of generating crystal structures that broadly correspond to the PXRD spectra. Although there is still room for improvement in these generated structures, they can provide experts in related fields with a highly viable crystal structures as candidates.

Table 2: **Results on ranked structure generation.**

| Candidates Generation | Metrics | Number of Candidates | | | |
|-----------------------|-----------------------|----------------------|---------------|---------------|---------------|
| | | 1 | 3 | 5 | 10 |
| Random | Match Rate \uparrow | 50.00 | 77.5 | 90.0 | 92.5 |
| | RMSE \downarrow | 0.4650 | 0.4305 | 0.4276 | 0.4109 |
| Rank | Match Rate \uparrow | 58.75 | 86.25 | 87.5 | 95.0 |
| | RMSE \downarrow | 0.4580 | 0.4254 | 0.4053 | 0.3985 |

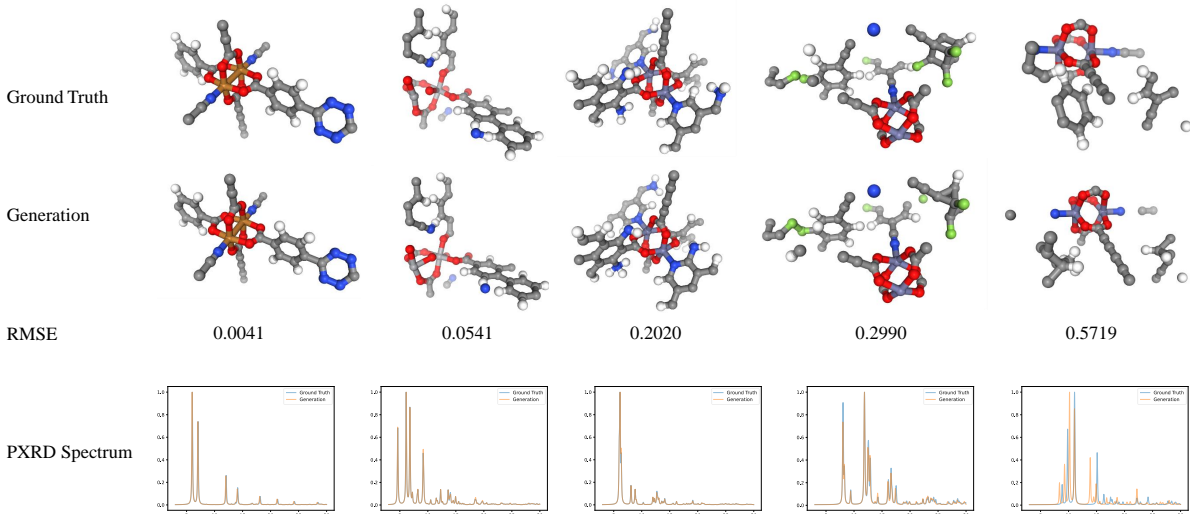


Figure 4: **Visualization of generation cases with different RMSEs.**

To provide a more intuitive understanding of the model’s generative capabilities, we select five generated samples for visualization. The corresponding ground truth structures, generated structures, and associated RMSE for these samples are displayed in Figure 4. We choose samples with varying RMSE to better illustrate the impact of different RMSE values on the quality of the generated results. It is apparent that the model performs well in generating the metal-connecting parts of the MOFs. The generated ligand structures are generally consistent with the ground truth structures, although the finer details is not perfect. Overall, the generated crystal structures have achieved a satisfactory level of accuracy.

2.5 Ablation Studies

We ablate several key components of XtalNet in Table 3. We first explore the impact of fusion type of PXRD features. If the PXRD features are treated as a new node in crystal structure network, the model suffers from extreme performance detriment, which may be caused by semantic difference between PXRD feature and atom feature. To verify the necessity of constrative learning pretraining of PXRD feature extractor, we construct a variant training all parameters from scratch, which results in a lower match rate. While freezing the PXRD encoder with pretrained parameters is also beneficial for the performance.

Table 3: **Ablation studies for ranked structure generation on hMOF-100 dataset.** **Top- k** denotes metrics are calculated on top k similarity score candidates. C denotes PXRD feature extractor has been pretrained by contrastive learning tasks. F denotes freezing PXRD feature extractor parameters during CCSG training process. P denotes the fusion type of PXRD feature, where *cat* denotes PXRD features are concatenate with node features, while *add* denotes PXRD features are added as a new node.

| Top-k | C | F | P | Match Rate \uparrow | RMSE \downarrow |
|---------------------------|---|---|-----|-----------------------|-------------------|
| 1 | | | add | 0.2375 | 0.5274 |
| | | | cat | 48.75 | 0.4106 |
| | ✓ | | cat | 63.75 | 0.4514 |
| | ✓ | ✓ | cat | 58.75 | 0.4580 |
| 3 | | | add | 35.0 | 0.5182 |
| | | | cat | 63.75 | 0.4023 |
| | ✓ | | cat | 77.5 | 0.4300 |
| | ✓ | ✓ | cat | 86.25 | 0.4254 |
| 5 | | | add | 43.75 | 0.5017 |
| | | | cat | 72.5 | 0.4076 |
| | ✓ | | cat | 85.0 | 0.4279 |
| | ✓ | ✓ | cat | 87.75 | 0.4053 |
| 10 | | | add | 55.0 | 0.4969 |
| | | | cat | 77.5 | 0.3990 |
| | ✓ | | cat | 92.5 | 0.4032 |
| | ✓ | ✓ | cat | 95.0 | 0.3985 |

3 Discussion

In conclusion, our methodology has convincingly demonstrated the feasibility of generating and predicting material structures under PXRD conditions. The successful application of our approach not only establishes a robust framework for the structural characterization in this specific context but also holds significant implications for material generation under a variety of other conditions. The implications of our findings extend beyond the immediate realm of PXRD, potentially informing and enhancing the predictive models used in different experimental and computational scenarios. Thus, our work not only contributes to the advancement of PXRD analysis but also serves as a valuable reference point for further research into the generalized prediction and synthesis of materials across diverse scientific disciplines.

4 Methods

The unit cell constitutes the fundamental repeating unit that serves as the basic building block for characterizing 3D crystal structures. A unit cell can be defined as $\mathcal{M} = (\mathbf{A}, \mathbf{F}, \mathbf{L})$, where $\mathbf{A} \in \mathbb{R}^N$ denotes atom types, $\mathbf{F} \in [0, 1)^{3 \times N}$ consists of fractional coordinates of the atoms, and $\mathbf{L} \in \mathbb{R}^{3 \times 3}$ represents the lattice matrix containing three basic vectors to describe the periodicity of the crystal. When a PXRD pattern \mathbf{C}_{XRD} is provided, based on prior knowledge, we can assume that both \mathbf{A} and N are given. Therefore, conditional CSP is to learning the conditional distribution $p(\mathbf{L}, \mathbf{F} \mid \mathbf{A}, \mathbf{C}_{XRD})$.

Our methodology combines two specialized neural networks to handle dual tasks involving PXRD and crystal structure data. We employ a PXRD Feature Extractor for identifying key PXRD features and a Crystal Structure Network for analyzing and generating crystal structures, including details such as lattice parameters and fractional atomic positions. The first task is to align PXRD and crystal structure data using a contrastive learning approach, similar to CLIP [16]’s method for images and text. The second task focuses on generating crystal structures based on features predicted by the PXRD Feature Extractor.

4.1 Model Architecture

PXRD Feature Extractor To identify patterns in PXRD data, we have developed a neural network, designated as the PXRD Feature Extractor (f_{PXRD}), based on the advanced transformer architecture. PXRD data is represented as curves with the diffraction angle on the x-axis and intensity on the y-axis. Given that peaks in PXRD data are of paramount importance compared to other regions, our analytical approach is tailored to prioritize these peaks, characterized by

their specific 2θ angle $\mathbf{A}_{xrd} \in \mathbb{R}^L$ and magnitudes $\mathbf{I}_{xrd} \in \mathbb{R}^L$. By strategically focusing on peak data, we effectively truncate the length of the data sequences. In our methodology, since \mathbf{A}_{xrd} is discrete and indicates the position of a peak, we interpret \mathbf{A}_{xrd} as position in traditional transformer while an embedding layer is employed to transform it into positional embedding. As the magnitudes \mathbf{I}_{xrd} is continuous, we use multilayer perceptron (MLP) networks to transform it into input token sequence. Further enhancing the analysis, a unique trainable PXRD token is prepended to the beginning of the tokenized sequences before they are input into the canonical transformer model for further processing. The post-transformation PXRD token embedding, $\mathbf{P} = f_{PXRD}(\mathbf{A}_{xrd}, \mathbf{I}_{xrd})$, is then employed as the embedding of the whole PXRD data for contrastive pretraining and the condition for diffusion models. The PXRD feature extractor is pretrained in CPCP module, while it is initialized by pretrained parameters and frozen in CCSG module.

Crystal Structure Network In our research, we adapt a Modified Equivariant Graph Neural Network (EGNN), called CSPNet [9], from the DiffCSP framework to serve as the Crystal Structure Network (f_{CSP}), leveraging its proven competence in processing crystallographic data. To align the model with our unique research objectives, we have instituted several alterations. Originally, the CSPNet constructed node representations by amalgamating node and temporal features, subsequently undergoing a linear transformation to generate the ultimate node features. Pertinent to the diffusion process, we have incorporated an additional supervisory signal absent in the original CSPNet. This is achieved by fusing the node features with both temporal and condition-specific PXRD features before subjecting them to a linear layer, thus deriving the final node representations.

$$\mathbf{I}_{node} = \text{Linear}(\mathbf{P}, t, \text{Embeddin}(\mathbf{A})) \text{ or } \text{Embeddin}(\mathbf{A})$$

$$\mathbf{C}, \hat{\varepsilon}_{\mathbf{F}}, \hat{\varepsilon}_{\mathbf{L}} = f_{CSP}(\mathbf{I}_{node}, \mathbf{F}, \mathbf{L}),$$

Where \mathbf{P} denotes PXRD feature, t denotes time embedding, \mathbf{C} denotes crystal feature, $\varepsilon_{\mathbf{F}}$ denoising term on fractional coordinate and $\varepsilon_{\mathbf{L}}$ denotes denoising term on lattice, while \mathbf{P} and t is the optional inputs. Within our contrastive learning paradigm, we employ the mean of final all node features to obtain crystal feature \mathbf{C} , which encapsulates the aggregate structural characteristics.

The pretrained PXRD feature extractor imparts conditional PXRD information that steer the direction of the crystal structure denoising. The PXRD features serve as a guide throughout this procedure, ensuring the synthesized crystal structure is not only in agreement with the PXRD data but also conforms to the material system’s intrinsic physical and chemical properties. This strategic enhancement integrates critical supervisory data into the model’s architecture.

4.2 Loss Functions

Contrastive Learning Loss We propose a contrastive learning framework designed to synergize two heterogeneous data types: PXRD patterns and crystal structures. This framework draws inspiration from the Contrastive Language-Image Pretraining (CLIP) approach, which effectively bridges the gap between visual and textual information. Our aim is to construct a joint embedding space in which the representations of PXRD and crystal data are cohesively aligned. This facilitates cross-modal correlations and bolsters the feature learning process. To achieve this, we employ the InfoNCE loss within each batch to attract paired modal data points while repulsing unpaired ones. The intended outcome is to obtain embeddings for both modalities that can accurately encapsulate the characteristics of the objects.

In the context of contrastive learning, the InfoNCE loss is defined as follows, τ is the temperature coefficient used to scale the similarity computation, \mathbf{P}_i is the i th PXRD feature and \mathbf{C}_i is the i th crystal structure feature.

$$\mathcal{L}_c = - \sum_{i=1}^N \log \frac{e^{\text{sim}(\mathbf{P}_i, \mathbf{C}_i)/\tau}}{\sum_{j=1}^N e^{\text{sim}(\mathbf{P}_i, \mathbf{C}_j)/\tau}} - \sum_{i=1}^N \log \frac{e^{\text{sim}(\mathbf{C}_i, \mathbf{P}_i)/\tau}}{\sum_{j=1}^N e^{\text{sim}(\mathbf{C}_i, \mathbf{P}_j)/\tau}} \quad (1)$$

$$\text{sim}(\mathbf{P}_i, \mathbf{C}_i) = \frac{\mathbf{P}_i \cdot \mathbf{C}_i}{\|\mathbf{P}_i\| \|\mathbf{C}_i\|}$$

Diffusion-Based Conditional Crystal Structure Generation Loss Our research methodology focuses on the generation of crystal structures through a diffusion-based generative framework, leveraged by conditioning on PXRD features derived from the PXRD Feature Extractor. Utilizing the Crystal Structure Network as the backbone of generative model, this approach integrates the PXRD features to guide an iterative refinement process. The whole diffusion framework is based on DiffCSP [9], the objective loss function is almost the same and we briefly describe it below.

For diffusion on lattice, the initial distribution can be defined as $p(\mathbf{L}_T) = \mathcal{N}(0, \mathbf{I})$ and the diffusion forward process $q(\mathbf{L}_t|\mathbf{L}_{t-1}) = \mathcal{N}(\mathbf{L}_t|\sqrt{1-\beta_t}\mathbf{L}_0, \mathbf{I})$ aims to add small gaussian noise into \mathbf{L}_{t-1} at time $t-1$, where $\beta_t \in (0, 1)$ control the variance. The lattice distribution at time t can be derived as the probability conditional on the initial distribution:

$$q(\mathbf{L}_t|\mathbf{L}_0) = \mathcal{N}(\mathbf{L}_t|\sqrt{\bar{\alpha}_t}\mathbf{L}_0, (1-\bar{\alpha}_t)\mathbf{I})$$

where $\bar{\alpha}_t = \prod_{s=1}^t \alpha_s = \prod_{s=1}^t (1-\beta_s)$ can be obtained by the cosine scheduler [21].

The reverse process is given by:

$$p(\mathbf{L}_{t-1}|\mathbf{M}_t) = \mathcal{N}(\mathbf{L}_{t-1}|\mu(\mathcal{M}_t), \sigma^2(\mathcal{M}_t)\mathbf{I}),$$

where $\mu(\mathcal{M}_t) = \frac{1}{\sqrt{\bar{\alpha}_t}}(\mathbf{L}_t - \frac{\beta_t}{\sqrt{1-\bar{\alpha}_t}}\varepsilon_{\mathbf{L}})$, $\sigma^2(\mathcal{M}_t) = \beta_t \frac{1-\bar{\alpha}_t-1}{1-\bar{\alpha}_t}$. The denoising term $\hat{\varepsilon}_{\mathbf{L}} \in \mathbb{R}^{3 \times 3}$ is predicted by f_{CSP} . For model training, the loss function of denoising lattice is defined as:

$$\mathcal{L}_{\mathbf{L}} = \mathbb{E}_{\varepsilon_{\mathbf{L}} \sim \mathcal{N}(0, \mathbf{I}), t \sim \mathcal{U}(1, T)} [\|\varepsilon_{\mathbf{L}} - \hat{\varepsilon}_{\mathbf{L}}\|_2^2]. \quad (2)$$

For diffusion on fractional coordinate, the distribution at time t can also be obtained by $\mathbf{F}_t = w(\mathbf{F}_0 + \sigma_t \boldsymbol{\epsilon}_{\mathbf{F}})$, where the truncation function $w(\cdot)$ is defined as $w(\mathbf{F}) = \mathbf{F} - \lfloor \mathbf{F} \rfloor \in [0, 1)^{3 \times N}$, $\boldsymbol{\epsilon}_{\mathbf{F}} \in \mathbb{R}^{3 \times N}$ is sampled from $\mathcal{N}(0, \mathbf{I})$ and σ_t is the noise scale which obeys the exponential scheduler: $\sigma_0 = 0$ and $\sigma_t = \sigma_1 (\frac{\sigma_T}{\sigma_1})^{\frac{t-1}{T-1}}$, if $t > 0$. The whole process contains the Wrapped Normal (WN) transition [22]:

$$q(\mathbf{F}_t|\mathbf{F}_0) \propto \sum_{\mathbf{Z} \in \mathbb{Z}^{3 \times N}} \exp\left(-\frac{\|\mathbf{F}_t - \mathbf{F}_0 + \mathbf{Z}\|_{\mathbf{F}}^2}{2\sigma_t^2}\right).$$

The reverse process is achieved by the ancestral predictor [23, 24] with the Langevin corrector [25], while the $\hat{\varepsilon}_{\mathbf{F}}$ is generated by f_{CSP} . Hence, the loss function of denoising fractional coordinate is defined as:

$$\mathcal{L}_{\mathbf{F}} = \mathbb{E}_{\mathbf{F}_t \sim q(\mathbf{F}_t|\mathbf{F}_0), t \sim \mathcal{U}(1, T)} [\lambda_t \|\nabla_{\mathbf{F}_t} \log q(\mathbf{F}_t|\mathbf{F}_0) - \hat{\varepsilon}_{\mathbf{F}}\|_2^2], \quad (3)$$

where $\lambda_t = \mathbb{E}_{\mathbf{F}_t}^{-1} [\|\nabla_{\mathbf{F}_t} \log q(\mathbf{F}_t|\mathbf{F}_0)\|_2^2]$ is approximated via Monte-Carlo sampling, which is detailed in [9].

4.3 Implementation Details

The training of both the PXRD feature extractor and the Crystal Structure Extractor follows a rigorous protocol. We use a batch size of 64 and employ the Adam optimizer with a learning rate of 1e-4 and cosine-decay scheduler. The models are trained on hMOF-100, a dataset of synthesized PXRD patterns and their corresponding crystal structures. The networks are implemented in PyTorch and trained on NVIDIA V100 GPUs for 400 epochs with 40 epochs warmup for both database contrastive learning task and conditional crystal structure generation task.

The combination of these methodological components and training regimens ensures the robustness and accuracy of our approach in extracting and refining crystal structures from PXRD data. The results, as we shall demonstrate, provide compelling evidence of the effectiveness of integrating advanced neural network architectures with material science domain knowledge.

5 Data and Code Availability Statements

Upon publication, we will make both the dataset and the codebase used in this study publicly available. This action is taken to facilitate reproducibility of the results, enable further research by the academic community, and enhance the integrity of the scientific process.

References

- [1] W. H. Zachariasen. A general theory of x-ray diffraction in crystals. *Acta Crystallographica*, 23:558–564, 1967.
- [2] Alec Belsky, Mariette Hellenbrandt, Vicky Karen, and Peter Luksch. New developments in the inorganic crystal structure database (icsd): Accessibility in support of materials research and design. *Acta crystallographica. Section B, Structural science*, 58:364–9, 07 2002.

- [3] H. M. Rietveld. A profile refinement method for nuclear and magnetic structures. *Journal of Applied Crystallography*, 2:65–71, 1969.
- [4] Woon Park, Jiyong Chung, Jaeyoung Jung, Keemin Sohn, Satendra Singh, Myoungho Pyo, Namsoo Shin, and Kee-Sun Sohn. Classification of crystal structure using a convolutional neural network. *IUCrJ*, 4, 06 2017.
- [5] Felipe Oviedo, Zekun Ren, Shijing Sun, Charlie Settens, Zhe Liu, Noor Titan Putri Hartono, Ramasamy Savitha, Brian L. DeCost, Siyu I. P. Tian, Giuseppe Romano, Aaron Gilad Kusne, and Tonio Buonassisi. Fast and interpretable classification of small x-ray diffraction datasets using data augmentation and deep neural networks, 2019.
- [6] Yuta Suzuki, Hideitsu Hino, Takafumi Hawaii, Kotaro Saito, Masato Kotsugi, and Kanta Ono. Symmetry prediction and knowledge discovery from x-ray diffraction patterns using an interpretable machine learning approach. *Scientific Reports*, 10, 12 2020.
- [7] Walter Kohn and Lu J. Sham. Self-consistent equations including exchange and correlation effects. *Physical Review*, 140:1133–1142, 1965.
- [8] Tian Xie, Xiang Fu, Octavian-Eugen Ganea, Regina Barzilay, and Tommi Jaakkola. Crystal diffusion variational autoencoder for periodic material generation, 2022.
- [9] Rui Jiao, Wenbing Huang, Peijia Lin, Jiaqi Han, Pin Chen, Yutong Lu, and Yang Liu. Crystal structure prediction by joint equivariant diffusion, 2023.
- [10] Ivano Castelli, David Landis, Kristian Thygesen, Søren Dahl, Ib Chorkendorff, Thomas Jaramillo, and Karsten Jacobsen. New cubic perovskites for one- and two-photon water splitting using the computational materials repository. *Energy & Environmental Science*, 5:9034, 10 2012.
- [11] Ivano Castelli, Thomas Olsen, Soumendu Datta, David Landis, Søren Dahl, Kristian Thygesen, and Karsten Jacobsen. Computational screening of perovskite metal oxides for optimal solar light capture. *Energy Environ. Sci.*, 5:5814, 02 2012.
- [12] Anubhav Jain, Shyue Ong, Geoffroy Hautier, Wei Chen, William Richards, Stephen Dacek, Shreyas Cholia, Dan Gunter, David Skinner, Gerbrand Ceder, and Kristin Persson. Commentary: The materials project: A materials genome approach to accelerating materials innovation. *APL Materials*, 1:011002, 07 2013.
- [13] Tian Xie, Xiang Fu, Octavian-Eugen Ganea, Regina Barzilay, and Tommi Jaakkola. Crystal diffusion variational autoencoder for periodic material generation. 2021.
- [14] Chris J. Pickard. Airss data for carbon at 10gpa and the c+n+h+o system at 1gpa, 2020.
- [15] Robin Rombach, Andreas Blattmann, Dominik Lorenz, Patrick Esser, and Björn Ommer. High-resolution image synthesis with latent diffusion models. *CoRR*, abs/2112.10752, 2021.
- [16] Alec Radford, Jong Wook Kim, Chris Hallacy, Aditya Ramesh, Gabriel Goh, Sandhini Agarwal, Girish Sastry, Amanda Askell, Pamela Mishkin, Jack Clark, Gretchen Krueger, and Ilya Sutskever. Learning transferable visual models from natural language supervision. *CoRR*, abs/2103.00020, 2021.
- [17] Christopher E Wilmer, Michael Leaf, Chang Yeon Lee, Omar K Farha, Brad G Hauser, Joseph T Hupp, and Randall Q Snurr. Large-scale screening of hypothetical metal–organic frameworks. *Nature chemistry*, 4(2):83–89, 2012.
- [18] Jingqi Wang, Jiapeng Liu, Hongshuai Wang, Guolin Ke, Linfeng Zhang, Jianzhong Wu, Zhifeng Gao, and Diannan Lu. Metal-organic frameworks meet uni-mof: a revolutionary gas adsorption detector. 2023.
- [19] Brian H Toby and Robert B Von Dreele. Gsas-ii: the genesis of a modern open-source all purpose crystallography software package. *Journal of Applied Crystallography*, 46(2):544–549, 2013.
- [20] Shyue Ping Ong, William Davidson Richards, Anubhav Jain, Geoffroy Hautier, Michael Kocher, Shreyas Cholia, Dan Gunter, Vincent L Chevrier, Kristin A Persson, and Gerbrand Ceder. Python materials genomics (pymatgen): A robust, open-source python library for materials analysis. *Computational Materials Science*, 68:314–319, 2013.
- [21] Alexander Quinn Nichol and Prafulla Dhariwal. Improved denoising diffusion probabilistic models. In *International Conference on Machine Learning*, pages 8162–8171. PMLR, 2021.
- [22] Valentin De Bortoli, Emile Mathieu, Michael John Hutchinson, James Thornton, Yee Whye Teh, and Arnaud Doucet. Riemannian score-based generative modelling. In Alice H. Oh, Alekh Agarwal, Danielle Belgrave, and Kyunghyun Cho, editors, *Advances in Neural Information Processing Systems*, 2022.
- [23] Jonathan Ho, Ajay Jain, and Pieter Abbeel. Denoising diffusion probabilistic models. *Advances in Neural Information Processing Systems*, 33:6840–6851, 2020.
- [24] Yang Song, Jascha Sohl-Dickstein, Diederik P Kingma, Abhishek Kumar, Stefano Ermon, and Ben Poole. Score-based generative modeling through stochastic differential equations. *arXiv preprint arXiv:2011.13456*, 2020.
- [25] Yang Song and Stefano Ermon. Improved techniques for training score-based generative models. *Advances in neural information processing systems*, 33:12438–12448, 2020.